

Study of one-dimensional of W/SiO₂ grating selective thermal emitter for thermophotovoltaic applications

Faustin Hilaire Tchoffo¹, Fabrice Kwefeu Mbakop^{1*}, Noël Djongyang¹

¹ Department of Renewable Energy, National Advanced School Of Engineering, University of Maroua (UMA), Maroua, Cameroon

² Department Renewable Energy and Energy Performance, Higher Institute of Agriculture, Forestry, Water and Environment (ISABEE) University of Ebolowa (UEb) Ebolowa, Cameroon

*Corresponding author E-mail: mbakop.fabrice@yahoo.fr

Abstract

In this paper, a one-dimensional multilayer is optimized for potential applications as thermophotovoltaic (TPV) selective emitter. The effect of the diffraction orders and plane of incidence on the spectral emittance of the proposed TPV emitter is calculated numerically by using the rigorous coupled-wave analysis (RCWA). The emittance spectrum of the proposed TPV selective emitter shows three close to unity emission peaks which are explained by the surface plasmon polariton (SPP), gap plasmon polariton (GPP) and magnetic polariton (MP) excitation. The strong emittance at short wavelengths occurs due to three peaks, one close to unity at 1.2 μ m wavelength, and two equal to unity at 0.8 and 1.59 μ m wavelengths. The proposed structure can be used as a selective emitter for TPV applications.

Keywords: Thermophotovoltaic; Selective Emitter; Rigorous Coupled Wave Analysis (RCWA); surface plasmon polaritons.

1. Introduction

Similar to a solar cell, in which the solar radiation is converted into electricity, a TPV cell converts the thermal radiation into electricity. The optical-to-electricity conversion is based on the photocurrent generation by those photons having energy exceeding the electronic band gap [1], [2]. A TPV system requires two key components: an emitter that gives out radiation by receiving the thermal energy from various heating sources, and a TPV cell that can generate electricity by the absorbing incident photons from the emitter [3]. The efficiency of this process depends critically on the selective emitter, which can be controlled by both the choice of material and the emitter design [4]. The PV cell absorbs the photons having energy greater than the cell bandgap energy and generates electron hole pairs that can be collected as a current through a connected load [5-7]. The emitter temperature in a TPV system generally ranges between 1000 and 2000 K. According to Wien's displacement law, this is optimum to PV cell with a band gap between 0.5 and 0.75 eV. Considering for instance the case of GaSb, which has a low- direct band gap energy about 0.7 eV, the optimum emitter temperature is about 1600 K, corresponding to a wavelength of 1.78 μ m. This makes it a good choice for a TPV system which transfers the photon energy into electricity [8-14]. The works carried out by Fraas et al. [9] have shown that in the high temperature category, silicon cells can be used with porous rare earth oxide selective emitters operating at over 1400°C [13], [15]. However, Near-field thermal radiation has been proposed to enhance the power generation by bringing the emitter and receiver in close proximity, [16-18] while the conversion efficiency can be improved by controlling the emission spectrum and directions. An ideal emitter should have emittance as high as possible above the bandgap and as low as possible below the bandgap (wavelength-selective) over the whole hemisphere, i.e., insensitive to the direction (diffuse-like). A number of microstructures have been studied to improve the performance of TPV emitters based on different physical mechanisms, such as one-dimensional (1D) complex grating, [19] 1D photonic crystal (PC) made of tungsten and alumina, [20] 2D tungsten grating with thermally excited surface plasmon polariton (SPPs), [21] 2D deep microcavities with cavity resonance modes, [22] and 3D woodpile-like PC. [23] Tungsten is usually selected as the emitter material due to high melting point and good corrosion resistance. On the other hand, the use of periodic structures such as metamaterials [24, 25] and photonic crystals [26, 27] has been shown to modify the emittance spectrum of selective emitters. Due to their simplicity and ease of fabrication, gratings are a promising practical option. Chen and Zhang [28] studied complex tungsten gratings, and showed that the excitation of surface plasmon polaritons (SPP) can greatly improve the thermal emittance. Song et al. [29, 30] proposed trilayer metal-insulator-metal (MIM) gratings made of W-SiO₂-W, and Shuai et al. [31] studied more general multilayer metal-dielectric gratings. Recently, multilayer W-HfO₂ metamaterial structures have been shown to enable thermal emission control through topological transitions [32-35]. In addition, Yeng et al. [36-38] filled a 2D tantalum photonic crystal with SiO₂ or HfO₂, and obtained omni-directional and polarization insensitive thermal emitters by exploiting cavity resonances. The HfO₂ dielectric in these structures appears promising for TPV applications due to its high melting point (3031 K).

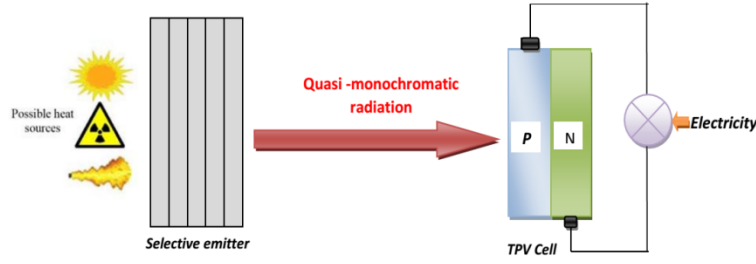


Fig. 1: Principle of Thermophotovoltaic Conversion.

2. Numerical method

Rigorous coupled-wave analysis (RCWA), formulated in the 1980s by Moharam and Gaylord, is used for analyzing the diffraction of electromagnetic waves by periodic gratings [39, 40]. It is used in this study to simulate the radiative properties (spectral emittance) of the periodically, micro-structured surfaces. It analyzes the diffraction problem by solving Maxwell's equations accurately in each of the three regions (input, multilayer, and output), based on Fourier expansion [41]. In RCWA, diffraction efficiency for each diffraction order is calculated with incident wave properties regardless of feature size, structural profiles, and dielectric function of the materials. The dielectric function of the materials is expressed as $\epsilon = (n + ik)^2$ where n is the refractive index and k is the extinction coefficient. The accuracy of the solution computed depends solely upon the number of terms retained in space harmonic expansion of electromagnetic fields, which corresponds to the diffraction order. The emittance is calculated from the reflectance according to Kirchhoff's law. Any linearly-polarized incidence can be decomposed into the transverse electric (TE) and transverse magnetic (TM) mode [40]. The normalized electric field of incidence can be expressed as: polarized incidence can be decomposed into the transverse electric (TE) and transverse magnetic (TM) mode. The normalized electric field of incidence E_{inc} can be expressed as:

$$E_{inc} = \exp(ik_x x + ik_z z - i\omega t) \quad (1)$$

The electric field in region I (Fig. 2a) is the superposition of the incident wave and the reflected waves; therefore [40]

$$E_I(x, z) = \exp(ik_x x + ik_z z) + \sum_j E_{rj} \exp(ik_{xj} x + ik_{zj}^t z) \quad (2)$$

Similarly, the electric field in region IV (E_{IV}) is the superposition of all transmitted waves

$$E_{IV}(x, z) = \sum_j E_{tj} \exp(ik_{xj} x + ik_{zj}^t z) \quad (3)$$

The magnetic field H in region I and IV can be obtained from Maxwell's equation

$$H_I(x, z) = -\frac{i}{\omega\mu_0} (\nabla \times E_I) \quad (4)$$

$$H_{IV}(x, z) = -\frac{i}{\omega\mu_0} (\nabla \times E_{IV}) \quad (5)$$

Where ω represents the frequency and μ_0 the magnetic permeability of vacuum. The electric and magnetic field components in region M (W/SO₂/W) (Fig2a) can be expressed as a Fourier series:

$$E_M(x, z) = \sum_j \chi_{yj}(z) \exp(ik_{xj} x) y \quad (6)$$

$$H_I(x, z) = -\frac{ik}{\omega\mu_0} \sum_j [\gamma_{xj}(z)x + \gamma_{zj}(z)z] \exp(ik_{xj} x) \quad (7)$$

Where χ_{yj} and γ_{xj} are vector components for the j^{th} space-harmonic electric and magnetic field in region M (multilayer region), respectively. ϵ_0 is the electric permittivity in vacuum. Due to the structure periodicity, the relative dielectric function in region M, $\epsilon(x)$ and its inverse, $\frac{1}{\epsilon(x)}$ can also be expanded in Fourier series:

$$\epsilon(x) = \sum_p \epsilon_p^{\text{ord}} \exp\left(i \frac{2p\pi}{\Lambda} x\right) \quad (8)$$

$$\frac{1}{\epsilon(x)} = \sum_p \epsilon_p^{\text{inv}} \exp\left(i \frac{2p\pi}{\Lambda} x\right) \quad (9)$$

Where ϵ_p^{ord} and ϵ_p^{inv} are the j^{th} Fourier coefficients for the ordinary and inverse of $\epsilon(x)$ respectively. [40]

3. Proposed structure

In this paper, we propose a structure made up of one-dimensional photonic crystals (LH)^N with N periods deposited on a substrate. For thermal energy transformation into electric power, the photovoltaic cell which operates perfectly in the infra-red is GaSb. Its gap energy is $E_g = 0.7\text{eV}$ and its gap wavelength is $\lambda_g = 1.78\mu\text{m}$. A 1D-PhCs is deposited on Si substrate which also serves as front encapsulation glass to a GaSb cell, separated from the emitter by 1 cm [5]. The proposed structure consists of grating layer a top a substrate, as shown

in Fig. 2(a) and (b). The grating period is $\Lambda = 600$ nm, the thickness of tungsten grating or silver lattice is $h = 30$ nm, the filling ratio $f = 0.40$, the thickness of SiO₂ spacer $d_1 = 100$ nm and the thickness of shallow tungsten layer $d_2 = 40$ nm. However to simulate the selective emitter explored here, Helmholtz's equation is solved by using the RCWA method [43-45] in order to find the reflectance (R). The absorptance (α) is calculated indirectly by energy conservation using $\alpha = 1 - R$. Finally, the emittance is obtained through Kirchhoff's law, which states that in thermal equilibrium the absorptance is equal to the emittance ($\alpha = \epsilon$) [43]. To obtain more realistic estimates of thermal emittance for selective emitters operating at high temperatures, the wavelength-dependent dielectric optical constants of tungsten, silver and silicon dioxide, in this work, are obtained from Palik et al [46]. The requirement of SPP excitation can be met by the incident radiation with a magnetic field component parallel to the grating vector (x-direction). In the present study, only transverse magnetic (TM) waves where the magnetic field is along the grating grooves is considered here since MPs cannot be excited for transverse electric waves (TE) in 1D grating structures. The waves are incident on the grating layer indicated by a wave vector k with an angle θ [16]. Optical constants for W/SiO₂ are obtained from tabulated data with interpolation.

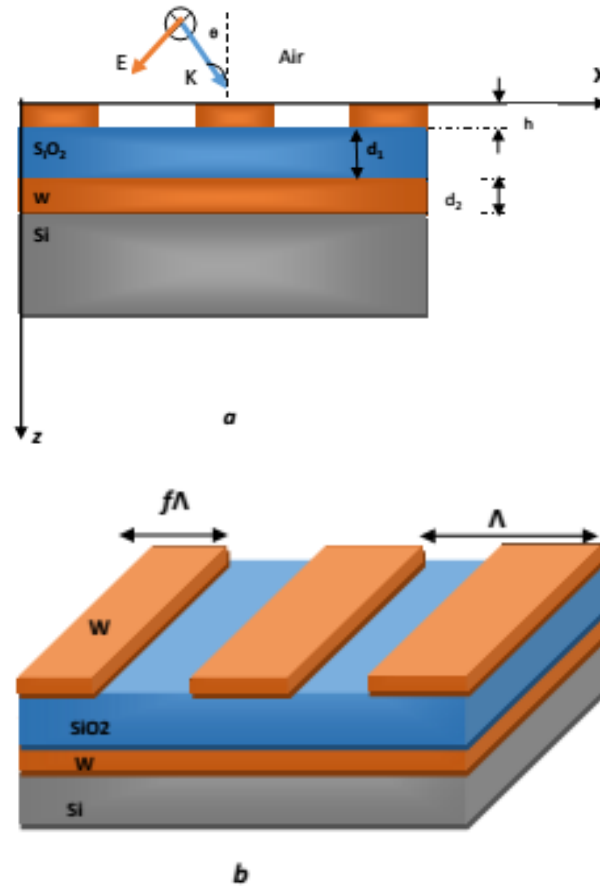


Fig. 2: (A) Basic Geometry Grating 1D Microstructure Selective Emitter, (B) Schematic of the Proposed A TPV Emitter Made of Multilayer Tungsten and Silicon Dioxide.

4. Results and discussion

4.1. The 1D presentation of the emittance of a simple network reinforced by a MP

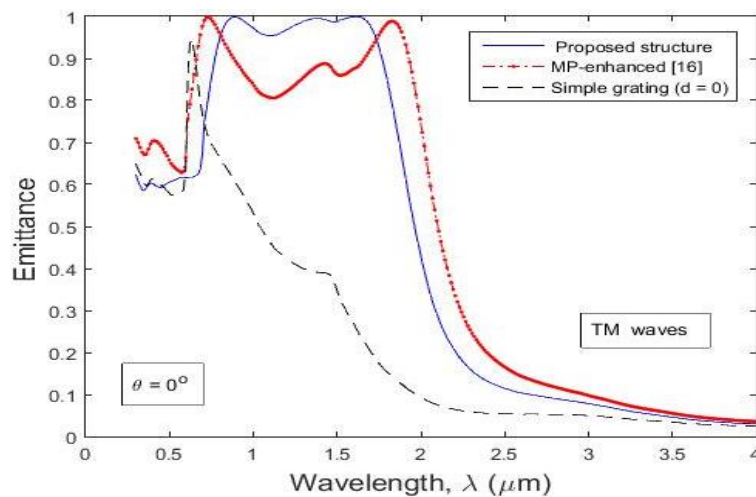


Fig. 3: Normal Emittance of Different TPV Emitters for TM Waves.

Figure 3 shows the calculated normal emittance spectrum (solid curve) of the proposed 1D selective emitter. As shown in this figure, the proposed emitter has a high emittance, above 0.92 and 0.98 in the broadband spectral ranges of 0.68-1.74 μm and 0.71-1.76 μm , respectively, but drops rapidly to less than 0.2 at long wavelengths above 2.1 μm . This is highly desirable for TPV applications in order to utilise short-wavelength photons as much as possible while minimising thermal leakage due to long-wavelength photons below the band gap of the TPV cell [16]. The strong emittance at short wavelengths occurs due to three peaks, one close to unity at 1.2 μm wavelength, and two equal to unity at 0.8 and 1.59 μm wavelengths. Comparing previous studies, the enhanced MP emittance of the structure presented by Zang [16] and Yaser [1] and the emittance for a single grating without the SiO₂ spacer are shown in Fig. 3. However, the single grating structure shows only one peak at the wavelength of 0.63 μm , due to the excitation of the SPP at the air-tungsten interface, but drops sharply as the wavelength increases. The resonance emittance for a single grating with no SiO₂ spacer is also shown (dashed curve) for comparison. This behaviour can be confirmed using the polariton dispersion relation [16]. The MPs are able to drive electrons or phonons with the magnetic field of incidence to generate antiparallel currents, which mediate the energy through the periodically corrugated surfaces so that the transmittance, absorptance, or both are enhanced by the reflectance reduction [28].

In this work, we propose like Yaser et al [1] a new 1D structure. In this structure the SiO₂ layer is sandwiched between the metal of the shallow lattice and the same metal layers of the shallow plane to further enhance the interaction between the SPP and the PMs. In the metal–dielectric–metal structure, a strong magnetic field enhancement (magnetic-plasmon resonance) exists inside the metal plates [48]. It is worth mentioning that, a minor emittance peak around 1.2 μm exists in the spectra of all three structures which is associated with interband absorption in tungsten.

4.2. The effect of dielectric thickness

The effect of the dielectric layer thickness d_1 on the emittance is shown in Figure 4.

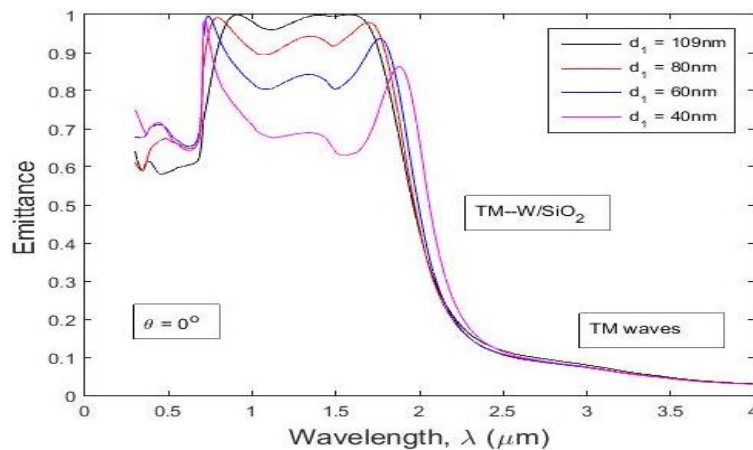


Fig. 4: Normal Emittance with Different D_1 Thickness, for TM Waves.

In Figure 4, we study the effect of the metal / dielectric thickness layer on the normal emittance of the proposed TPV emitter is investigated at different layer thicknesses. The effect of the thickness of the dielectric layer d_1 on the normal emittance is shown in Fig. 4. However, the results show us that the first and second peak move towards high wavelengths. When the thickness is varied from 40, 60, and 80, the third peak shifts towards short wavelengths as it approaches the second peak. The wavelengths corresponding to these different thicknesses are worth: 1.8 μm , 1.9 μm and 2 μm . Consequently, the bandwidth of the emittance becomes narrower. When the thickness of the dielectric layer d_1 is increased by 109nm, the second and the third peak are related to a normal emittance reaching almost 97% for a limiting wavelength of $\lambda = 1.7\mu\text{m}$. However, we retain that the first peak is attributed to the excitation of (SPP) and the second corresponds to the excitation coupling effect of the gap plasmon polaritons (GPP) and the third corresponds to excitation of the magnetic polaritons (MP). These results are in accordance with those obtained by Yaser et al [1].

4.3. The effect of the thickness of the metal layer on the emittance

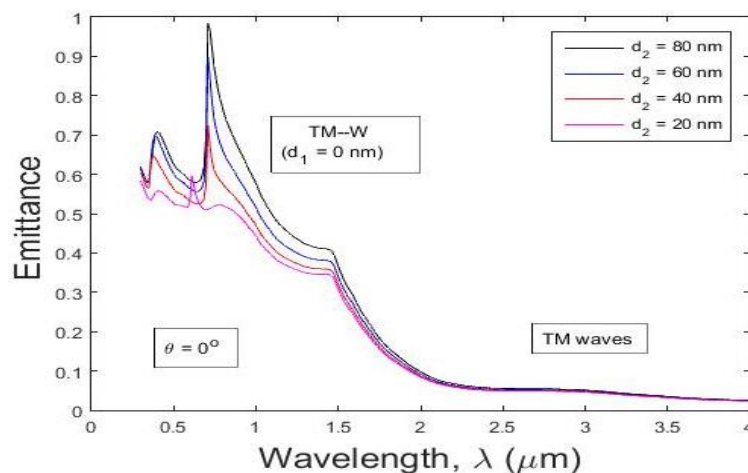


Fig. 5: The Effect of the Thickness of Metal.

On Figure 5 we present this time the effect of the variation of the thickness of the metal layer (W) of the normal emission for a simple lattice which has no SiO_2 spacer. Thus, the thickness of the spacer is equal to $d_1 = 0$. We observe in this figure that when we set the thickness at 20nm we have a very low value of the normal emittance corresponding to a wavelength of $0.5\mu\text{m}$. Consequently, the emittance gradually increases towards the long wavelengths when the values of the thickness vary from 40 to 60nm. However, we notice that the wavelength shift towards larger ones and have a similar wavelength which is $0.8\mu\text{m}$. Therefore, this wavelength remains unchanged for any thickness greater than 40nm. The maximum emissivity is reached when the layer thickness is 80nm.

4.4. Effect of the number of periods on the emittance

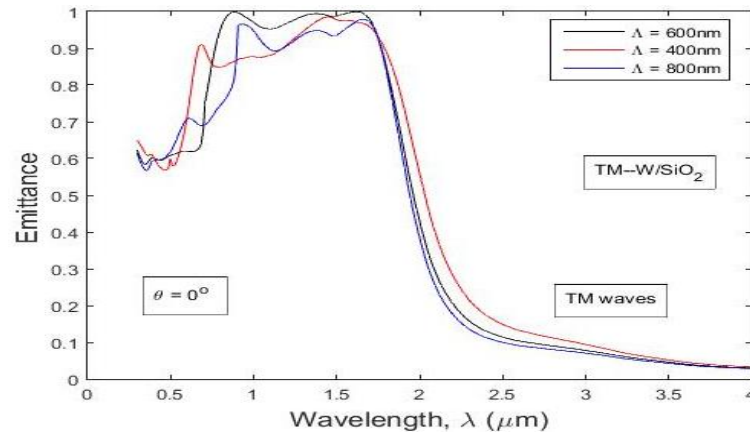


Fig. 6: Variation of the Period on Different Layers of the Emittance.

Figure 6 shows the behavior of the structure at different times. In Fig. 6, the first peak representing the SPP and the third peak that of the MPs are at the maximum value at 100% of the emissivity when the number of periods Λ increases from 400nm to 800nm. However, we observe a large bandwidth of the emissivity when we set the period at 400nm. Consequently, the SPP is located at the level of the short wavelengths having a value of $0.6\mu\text{m}$. GPPs has a higher peak than SPP. For this period, the MPs are almost non-existent. However, when we increase the period to 600nm, we have the first and the third peak of the emittance corresponding to the SPP and to the MPs which are worth 100%. This period corresponds to that of Fig. 3 which has a wavelength of $1.2\mu\text{m}$ and drops to $1.74\mu\text{m}$. Consequently, the emissivity decreases considerably and reaches a value of 95% for the SPP when the period is increased to 800nm. The combination of quasi-phase tuning and photonic band edge effects in a nonlinear structure with periodically polarized crystals can dramatically increase the conversion efficiency, often by three to four orders of magnitude over the use of a quasi-phase agreement only. The period of a nonlinear structure makes it possible to significantly increase the conversion efficiency [37]. However, the period corresponding to this study is 600nm.

4.5. The effect of diffraction orders

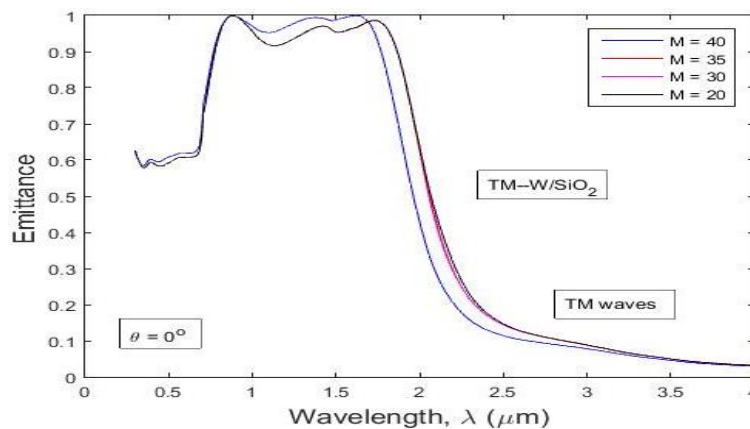


Fig. 7: Normal Emittance with Different Diffraction Orders for TM Waves.

The directional-hemispherical reflectance and transmittance can be obtained by summing up the diffraction efficiencies for all orders. All the transmitted energy is absorbed by the tungsten substrate and the emittance can be obtained as according to Kirchhoff's law $\epsilon = 1 - R$ where R the reflectance for given wavelength, incidence angle, and polarization. When light impinges onto the multilayer structure, it diffracts into different directions, depending on the wavelength and the layer period. The accuracy of the solution computed for emittance depends solely upon the number of the diffraction orders. However, the effect of the diffraction orders on the normal emittance of the proposed TPV emitter is also studied for the TM polarization [40, 48]. Therefore the results of Figure 7 show that the diffraction orders (M) hardly change when a values ranging from 20, 30 and 35. However, we notice that when we vary the diffraction until obtaining a value of 40 there is a change and an increase in normal emittance. Therefore, $M = 40$ is chosen in this study. The emittance spectrum is shown in Figure 3 matches well with the GaSb p-n junction TPV cell, which has a bandgap around $1.78\mu\text{m}$. As mentioned previously, a higher emittance at $\lambda > \lambda_g$ and lower emittance at $\lambda < \lambda_g$ is desired to improve the conversion efficiency for TPV systems. The effect of emittance at $\lambda < 30\text{nm}$ on the conversion efficiency is much weaker according to Planck's blackbody spectral distribution.

4.6. Effect of the plane of incidence

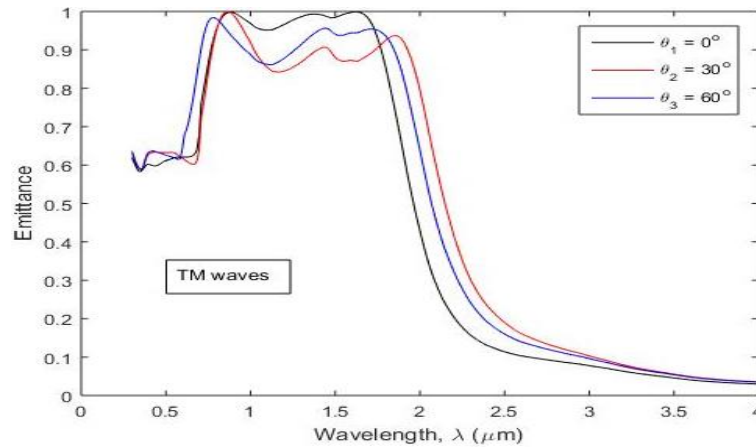


Fig. 8: Effect of the Plane of Incidence on the Spectral Emittance.

The effect of the plane of incidence on the spectral emittance of the proposed TPV emitter was studied numerically at different incidence angles for TM wave, as shown in Figure 8. The results show that there is hardly any change in the first emittance peak, but the second emittance peak disappears while the third peak moves toward shorter wavelengths, when the angle of incidence is increased from 0° to 60° [49]. It appears that the proposed TPV emitter is insensitive to direction and has high emittance value in near Define abbreviations and acronyms the first time they are used in the text, even after they have been defined infrared region, so it can be suitable to be used as a wavelength selective emitter in TPV systems.

5. Conclusion

The present study we have studied a structure consisting of 1D microstructure tungsten (gratings), for design and development of a spectrally selective emitters that are to be used in TPV applications. The effect of geometric parameters on the spectral emittance is investigated by Rigorous Coupled-Wave Analysis (RCWA) method.

The proposed emitter has a high emittance, above 0.92 and 0.98 in the broadband spectral ranges of $0.68\text{-}1.74\mu\text{m}$ and $0.71\text{-}1.76\mu\text{m}$, respectively. However, When the thickness is varied from 40, 60, and 80, the third peak shifts towards short wavelengths as it approaches the second peak. Theremore notice that when we vary the diffraction until obtaining a value of 40 there is a change and an increase in normal emittance

Nomenclature

TPV: Thermophovoltaic
TM : Magnetic polarization

TE: Electric polarization

VIS: Visible

IR: Infrared

PhCs : photonic crystal

1D: One-dimension

N: Period

R: Reflectance (%)

c: Velocity of light $c= 3.10^8\text{ m s}^{-1}$

Si: Silicon

T : Transmittance (%)

r: Fresnel reflection coefficient (%)

t: Fresnel transmission coefficient (%)

n_s : Refractive index of the substrate

n_o : The index of refraction of air

magnesium fluoride

l_k : Thickness of the layer k

l_{Si} : Thickness of the layer silicon

θ : Angle of incidence

λ_0 : Central wavelength (nm)

λ : Wavelength (nm)

μ_o : Permeability

ε_o : Dielectric constant

References

- [1] Y. Khorami, D. Fathi, "Broadband Thermophotovoltaic Emitter using Magnetic Polaritons based on Multilayer Structure", 27th Iranian Conference on Electrical Engineering (ICEE2019) <https://doi.org/10.1364/IOSAB.36.000662>.
- [2] S. Y. Lin, J. Moreno, and J. G. Fleming, "Three-dimensional photonic-crystal emitter for thermal photovoltaic power generation", *Appl. Phys. Lett.*, vol. 83, pp. 380-382, July 2003. <https://doi.org/10.1063/1.1592614>.
- [3] B. Zhao, L. Wang, Y. Shuai, Z. M. Zhang, "Thermophotovoltaic emitters based on a two-dimensional grating/thin-film nanostructure", *Int. J. Heat Mass Transf.*, vol. 67, pp. 637-645, August 2013. <https://doi.org/10.1016/j.ijheatmasstransfer.2013.08.047>.
- [4] Z. Zhou, Q. Chen, P. Bermel, "Prospects for high-performance thermophotovoltaic conversion efficiencies exceeding the Shockley–Queisser limit", *Energ. Convers. Manage.*, vol. 97, pp. 63-69, June 2015. <https://doi.org/10.1016/j.enconman.2015.03.035>.
- [5] F. K. Mbakop, A. Tom, A. Dadjé, C. V. K. Aloyem, N. Djongyang, "One-dimensional comparison of TiO₂/SiO₂ and Si/SiO₂ photonic crystals filters for thermophotovoltaic applications in visible and infrared", *Chinese Journal of Physics* 67 (2020) 124–134 <https://doi.org/10.1016/j.cjph.2020.06.004>.
- [6] V. Badescu, Thermodynamic theory of thermophotovoltaic solar energy conversion, *J. Appl. Phys.* 90 (2001) 6476–6486. <https://doi.org/10.1063/1.1415756>.
- [7] M. Zenker, A. Heinzl, G. Stollwerck, J. Ferber, J. Luther, Efficiency and power density potential of combustion-driven thermophotovoltaic systems using GaSb photovoltaic cells, *Electron Devices, IEEE Trans.* 48 (2001) 367e76. <https://doi.org/10.1109/16.902740>.

- [8] S. G. Babiker, S. Yong, M. O. Sid-Ahmed, X. Ming, "Thermophotovoltaic Emitters Based on a One-Dimensional Metallic-Dielectric Multilayer Nanostructures", *Journal of Electronics Cooling and Thermal Control*, 2014, 4, 39-48 <https://doi.org/10.4236/jectc.2014.41005>.
- [9] L.M. Fraas, J.E. Avery, H.X. Huang, R.U. Martinelli, Thermophotovoltaic system configurations and spectral control, *Semicond. Sci. Technol.* 18 (2003) S165–S173. <https://doi.org/10.1088/0268-1242/18/5/305>.
- [10] N.Z. Jovanovic, "Two-dimension photonic crystals as selective emitters for thermophotovoltaic power conversion applications", Thesis, Massachusetts Institute of Technology, (2005).
- [11] F.K. Mbakop, N. Djongyang, J.Y. Effa, D. Raïdandi, J.L.D.B. Nsouandélé, R. Tchinda, Assessment of the radiative properties of some semiconductors for applications in thermophotovoltaic and thermophotonic conversion systems, *Int. J. Basic Appl. Sci.* 3 (4) (2014) 401–413. <https://doi.org/10.14419/ijbas.v3i4.3261>.
- [12] C.Q. Zhang, Recent progress in high-temperature solar selective coatings, *Solar Energy Mater. Solar Cells* 62 (1–2) (2000) 63–74. [https://doi.org/10.1016/S0927-0248\(99\)00136-1](https://doi.org/10.1016/S0927-0248(99)00136-1).
- [13] K. Sharma, H.S. Zaidi, C.P. Logofatu, J.R.S. Breuck, Optical and electrical properties of nanostructured metal-silicon-metal photodetectors, *IEEE J. Quantum Electron.* 38 (12) (2002) 1651–1660. <https://doi.org/10.1109/JQE.2002.805112>.
- [14] L.C. Chia, B. Feng, The development of a micropower (micro-thermophotovoltaic) device (Review), *Power Sources* 165 (2007) 455–480. <https://doi.org/10.1016/j.jpowsour.2006.12.006>.
- [15] L. Mao, H. Ye, New development of one-dimensional Si/SiO₂ photonic crystals filter for thermophotovoltaic applications, *Renew Energy* 35 (2010) 249–256. <https://doi.org/10.1016/j.renene.2009.06.013>.
- [16] L. P. Wang, Z. M. Zhang, "Wavelength-selective and diffuse emitter enhanced by magnetic polaritons for thermophotovoltaics", *Applied Physics Letters* 100, 063902 (2012) <https://doi.org/10.1063/1.3684874>.
- [17] K. Park, S. Basu, W. P. King, Z. M. Zhang, "Performance analysis of near-field thermophotovoltaic devices considering absorption distribution" *J. Quantum Spectrosc Radiat. Transfer* 109, 305 (2008) <https://doi.org/10.1016/j.jqsrt.2007.08.022>.
- [18] M. Francoeur, R. Vaillon, M. P. Menguc, "Thermal impacts on the performance of nanoscale-gap thermophotovoltaic power generators" *IEEE Trans. Energy Convers.* 26, 686 (2011). <https://doi.org/10.1109/TEC.2011.2118212>.
- [19] Y.-B. Chen, Z. M. Zhang, "Design of tungsten complex gratings for thermophotovoltaic radiators" *Opt. Commun.* 269, 411 (2007) <https://doi.org/10.1016/j.optcom.2006.08.040>.
- [20] A. Narayanaswamy, G. Chen, "Thermal emission control with one-dimensional metallodielectric photonic crystals", *Phys. Rev. B* 70, 125101 (2004). <https://doi.org/10.1103/PhysRevB.70.125101>.
- [21] A. Heinzl, V. Boerner, A. Gombert, B. Blasi, V. Wittwer, J. Luther, "Radiation filters and emitters for the NIR based on periodically structured metal surfaces", *J. Mod. Opt.* 47, 2399 (2000). <https://doi.org/10.1080/09500340008230522>.
- [22] H. Sai, Y. Kanamori, H. Yugami, "Tuning of the thermal radiation spectrum in the near-infrared region by metallic surface microstructures" *J. Microchem. Microeng.* 15, S243 (2005). <https://doi.org/10.1088/0960-1317/15/9/S12>.
- [23] J.-H. Lee, Y.-S. Kim, K. Constant, K.-M. Ho, "Polarization engineering of thermal radiation using metallic photonic crystals," *Adv. Mater.* 19, 791 (2007). <https://doi.org/10.1002/adma.200602550>.
- [24] H. Deng, T. Wang, J. Gao, and X. Yang, "Metamaterial thermal emitters based on nanowire cavities for high-efficiency thermophotovoltaics," *J. Opt.* 16, 35102 (2014). <https://doi.org/10.1088/2040-8978/16/3/035102>.
- [25] H. Wang, J. Chang, Y. Yang, and L. Wang, "Performance analysis of solar thermophotovoltaic conversion enhanced by selective metamaterial absorbers and emitters," *Int. J. Heat Mass Transf.* 98, 788–798 (2016). <https://doi.org/10.1016/j.ijheatmasstransfer.2016.03.074>.
- [26] V. Rinnerbauer, A. Lenert, D. M. Bierman, Y. X. Yeng, W. R. Chan, R. D. Geil, J. J. Senkevich, J. D. Joannopoulos, E. N. Wang, M. Soljačić, and I. Celanovic, "Metallic Photonic Crystal Absorber-Emitter for Efficient Spectral Control in High-Temperature Solar Thermophotovoltaics," *Adv. Energy Mater.* 4, 1400334 (2014). <https://doi.org/10.1002/aenm.201400334>.
- [27] I. Celanovic, F. O'Sullivan, N. Jovanovic, M. Qi, and J. G. Kassakian, "1D and 2D Photonic Crystals for Thermophotovoltaic Applications," in *Photonic Crystal Materials and Nanostructures*, R. M. De La Rue, P. Viktorovitch, C. M. Sotomayor Torres, and M. Midrio, eds. (Photonic Crystal Materials and Nanostructures, 2004), Vol. 5450, pp. 416–422. <https://doi.org/10.1117/12.545539>.
- [28] Y.-B. Chen and Z. M. Zhang, "Design of tungsten complex gratings for thermophotovoltaic radiators," *Opt. Commun.* 269, 411–417 (2007). <https://doi.org/10.1016/j.optcom.2006.08.040>.
- [29] N. Nguyen-Huu, J. Pištora, and M. Cada, "Wavelength-selective emitters with pyramid nanogratings enhanced by multiple resonance modes," *Nanotechnology* 27, 155402 (2016). <https://doi.org/10.1088/0957-4484/27/15/155402>.
- [30] J. Song, H. Wu, Q. Cheng, and J. Zhao, "1D trilayer films grating with W/SiO₂/W structure as a wavelength-selective emitter for thermophotovoltaic applications," *J. Quant. Spectrosc. Radiat. Transf.* 158, 136–144 (2015). <https://doi.org/10.1016/j.jqsrt.2015.02.002>.
- [31] Y. Shuai, H. Tan, and Y. Liang, "Polariton-enhanced emittance of metallic-dielectric multilayer structures for selective thermal emitters," *J. Quant. Spectrosc. Radiat. Transf.* 135, 50–57 (2014). <https://doi.org/10.1016/j.jqsrt.2013.11.011>.
- [32] N. Nguyen-Huu, Y.-B. Chen and Y.-L. Lo, "Development of a polarization-insensitive thermophotovoltaic emitter with a binary grating," *Opt. Express* 20, 5882–5890 (2012). <https://doi.org/10.1364/OE.20.005882>.
- [33] Erwin G. Loewen and E. Popov, *Diffraction Gratings and Applications* (CRC Press, 1997).
- [34] P. N. Dyachenko, S. Molesky, A. Y. Petrov, M. Störmer, T. Krekeler, S. Lang, M. Ritter, Z. Jacob, and M. Eich, "Controlling thermal emission with refractory epsilon-near-zero metamaterials via topological transitions," *Nat. Commun.* 7, 11809 (2016). <https://doi.org/10.1038/ncomms11809>.
- [35] Y. X. Yeng, J. B. Chou, V. Rinnerbauer, Y. Shen, S.-G. Kim, J. D. Joannopoulos, M. Soljačić, and I. Celanovic, "Global optimization of omnidirectional wavelength selective emitters/absorbers based on dielectric-filled anti-reflection coated two-dimensional metallic photonic crystals," *Opt. Express* 22, 21711 (2014). <https://doi.org/10.1364/OE.22.021711>.
- [36] H. Padma Kumar, S. Vidya, S. Saravana Kumar, C. Vijayakumar, S. Solomon, and J. K. Thomas, "Optical properties of nanocrystalline HfO₂ synthesized by an auto-igniting combustion synthesis," *J. Asian Ceram. Soc.* 3, 64–69 (2015) <https://doi.org/10.1016/j.jascr.2014.10.009>.
- [37] F.K. Mbakop, N. Djongyang, D. Raïdandi, One-dimensional TiO₂/SiO₂ photonic crystal filter for thermophotovoltaic applications, *J. Euro. Opt. Soc. Rapid. Pub. Springer*, 2016. <https://doi.org/10.1186/s41476-016-0026-4>.
- [38] F.K. Mbakop, N. Djongyang, G.W. Ejuh, P. Wofo, D. Raïdandi, Transmission of light through an optical filter of a one-dimensional photonic crystal: application to the solar thermophotovoltaic system, *Phys. B, Elsevier* 516 (2017) 92–99. <https://doi.org/10.1016/j.physb.2017.04.033>.
- [39] S. G. Babiker, Y. Shuai, M. O. Sid-Ahmed, M. Xie, "One-Dimensional Si/SiO₂ Photonic Crystals Filter for Thermophotovoltaic Applications", *Ws. Transactions On Applied And Theoretical Mechanics*, 2224-3429, Volume 9, 2014
- [40] G.S. Babiker, S. Yong, O. Mohamed, S. Ahmed, X. Ming, "One-dimensional multilayer microstructure emitter for thermophotovoltaic applications", *Int. J. Energy, Inf. Commun.* 5 (1) (2014) 9–20. <https://doi.org/10.14257/ijeic.2014.5.4.01>.
- [41] S. Peng, G. M. Morris, "Efficient implementation of rigorous coupled-wave analysis for surface-relief gratings", *Opt. Soc. Am. A*, vol. 12, no. 5, (1995), pp. 1087-1096 <https://doi.org/10.1364/JOSAA.12.001087>.
- [42] M. G. Moharam, T. K. Gaylord, "Rigorous coupled-wave analysis of planar-grating diffraction", *Opt. Soc. Am.*, vol. 71, no. 7, (1981), pp. 811-818. <https://doi.org/10.1364/JOSA.71.000811>.
- [43] G. S. Elker, C. J. E. H. Anckes, P. Fay, "Study of W/HfO₂ grating selective thermal emitters for thermophotovoltaic applications", *Opt. Express*, Vol. 26, No. 22 (2018). <https://doi.org/10.1364/OE.26.00A929>.
- [44] Z. M. Zhang, *Nano/Micro Scale Heat Transfer* (McGraw-Hill, 2007).
- [45] M. Moharam and T. Gaylord, "Rigorous coupled-wave analysis of planar-grating diffraction," *J. Opt. Soc. A* 71, 811 (1981). <https://doi.org/10.1364/JOSA.71.000811>.
- [46] E. D. Palik, "Handbook of Optical Constants of Solids", Academic Press. San Diego, CA, (1985)

- [47] S. Wu, G. D. Wang, Q. J. Wang, L. Zhou, J. W. Zhao, C. P. Huang, and Y. Y. Zhu, "Novel optical transmission property of metal-dielectric multilayered structure," *J. Phys. D* 42, 225406 (2009). <https://doi.org/10.1088/0022-3727/42/22/225406>.
- [48] S. Basu, Y. -B. Chen, Z. M. Zhan, "Microscale radiation in thermophotovoltaic devices - A review", *Int. J. Energy Res*, vol. 31, pp. 689-716 (2007). <https://doi.org/10.1002/er.1286>.
- [49] S. G. Babiker, S. Yong, M. O. S. Ahmed, X. Ming, "Thermophotovoltaic Emitters Based on a One-Dimensional Metallic-Dielectric Multilayer Nanostructures" *Journal of Electronics Cooling and Thermal Control*, 4, 39-48. (2014). <https://doi.org/10.4236/jectc.2014.41005>.